Anionic sulfonated and carboxylated PPI dendrimers with the EDA core: Synthesis and characterization of selective metal complexing agents

ARTICLE *in* DALTON TRANSACTIONS · MARCH 2013

Impact Factor: 4.2 · DOI: 10.1039/c3dt32870h · Source: PubMed

8 AUTHORS, INCLUDING:

Michela Cangiotti
Università degli Studi di Urbino "Carlo Bo"
44 PUBLICATIONS **330** CITATIONS
SEE PROFILE

Luigi Fiorani
Università degli Studi di Urbino "Carlo Bo"
6 PUBLICATIONS **37** CITATIONS
SEE PROFILE

Alberto Fattori
Università degli Studi di Urbino "Carlo Bo"
12 PUBLICATIONS **93** CITATIONS
SEE PROFILE

Maria Angeles Muñoz-Fernández
Hospital General Universitario Gregorio Ma…
424 PUBLICATIONS **5,888** CITATIONS
SEE PROFILE

Dalton Transactions

RSC Publishing

PAPER

View Article Online
View Journal | View Issue

Cite this: *Dalton Trans.*, 2013, **42**, 5874

Anionic sulfonated and carboxylated PPI dendrimers with the EDA core: synthesis and characterization of selective metal complexing agents†

Sandra García-Gallego,[a,b] Michela Cangiotti,[c] Luigi Fiorani,[c] Alberto Fattori,[c] M[a] Ángeles Muñoz-Fernández,[b,d] Rafael Gomez,[a,b] M. Francesca Ottaviani*[c] and F. Javier de la Mata*[a,b]

Herein we describe the synthesis and characterization of new sulfonated and carboxylated poly(propyleneimino) (PPI) dendrimers with the ethylenediamino (EDA) core, at generations 1, 2 and 3. By means of UV-Vis and EPR spectroscopy, using Cu^{2+} as a probe, we concluded that these dendrimers show a specific pattern in the coordination of metal ions. In agreement with the UV-Vis studies, EPR spectra of carboxylated compounds are constituted by 3 different signals which appear and then disappear with increasing copper concentration, corresponding to the saturation of different copper complexation sites. At the lowest copper concentration up to a 1 : 1 molar ratio between Cu^{II} and the dendrimer, the spectrum is characteristic of a CuN_2O_2 coordination at the core of the dendrimer. The spectrum appearing at higher Cu^{II} concentrations indicates a peripheral location of the ions coordinating one nitrogen and 3 oxygen atoms in a square planar geometry in restricted mobility conditions. For the highest concentrations tested, copper ions are confined at the external dendrimer surface with CuO_4 coordination. For sulfonate systems, the EPR results are in line with a weaker interaction of Cu^{II} with the nitrogen sites and a stronger interaction with the oxygen (SO_3^-) groups with respect to the interactions measured by EPR for carboxylate systems.

Received 30th November 2012,
Accepted 7th February 2013

DOI: 10.1039/c3dt32870h

www.rsc.org/dalton

Introduction

Dendrimers are highly branched nanosystems with unique physical, chemical and biological properties, such as well-defined structure, monodispersity, structural control and multivalence. Their promising potential for applications in life and materials science encourages great research efforts in dendrimer chemistry.[1–3] A challenging aspect of dendrimer chemistry is the coordination of metal ions in different parts of their structure, such as the central core,[4] the interior and exterior branches[5,6] or the complexing units in the outer shell.[7] The resultant metallodendrimers present different properties from their parent dendrimers; for instance, poly(propyleneimine) dendrimers self-assemble into nanofibers[8] in the presence of Cd^{2+}, driven by the formation of multiple coordination bonds between the Cd^{II} cations and free primary amines at the dendrimer surface.

Poly(amidoamino) (PAMAM), poly(propyleneimine) (PPI) and poly(ethyleneimine) (PEI) dendrimers,[9] and their modified derivatives, have been widely studied due to their interesting physicochemical properties, such as biocompatibility, high water solubility, and terminal-modifiable amino functional groups. Moreover, they are especially attractive for binding metal ions in aqueous solution because of their controlled size and chelating behavior, and the availability of their internal tertiary amines and amide groups as binding sites for metal ions.[5,10–16] In the case of PAMAM dendrimers, a strong binding to Ni^{II}, Cu^{II} and Co^{II} has been demonstrated.[10,16–25] However, a metal ion with little or no ligand field stabilization, like Mn^{II}, does not bind to full generation PAMAM's at any pH while it binds half generation PAMAM dendrimers.[22] This behaviour is also observed for PEI and PPI dendrimers and hyperbranched polymers. Bosman and others[6,26] had previously described the complexation properties of unmodified G1 and G5 DAB-PPI against transition metal ions such as Cu^{II},

[a]*Departamento de Química Inorgánica, Universidad de Alcalá, Campus Universitario, E-28871 Alcalá de Henares, Spain*
[b]*Networking Research Center on Bioengineering, Biomaterials and Nanomedicine (CIBER-BBN), Spain. E-mail: javier.delamata@uah.es; Fax: (+34) 91 8854683; Tel: (+34) 91 8854654*
[c]*Department of Earth, Life and Environment Sciences, 61029 Urbino, Italy. E-mail: maria.ottaviani@uniurb.it*
[d]*Laboratorio de Inmunobiología Molecular, Hospital General Universitario Gregorio Marañón, Madrid, Spain. E-mail: mmunoz.hgugm@salud.madrid.org*
†Electronic supplementary information (ESI) available. See DOI: 10.1039/c3dt32870h

Zn^{II} and Ni^{II}, indicating an exclusive coordination of $n/2$ ions (n = generation) in the periphery in a tridentate fashion. By comparing with analogous dendrimers with amide groups at the periphery, where no complexation was observed, they postulate an absence of interaction of Cu^{II} with the inner tertiary amines. However, many other papers refuted this fact.[15,17,19,21]

The applications of such metallodendrimers comprise different fields; for instance, some PPI dendrimers coordinate metal ions such as Fe^{3+}, Co^{2+}, Cu^{2+}, VO^{2+}, *etc.*, and act as catalysts[27] in epoxidation of cyclohexene, or some complexes of Cu^{II}, Zn^{II} and Ni^{II} of different generations of DAB[6] have been used as support materials for metal nanoparticles in water. In the biomedical field, some metallodendrimers present interesting activities, such as antibacterial properties (Cu^{II} and Zn^{II} complexes of PPI dendrimers[28] comprising 1,8-naphthalimide units on the periphery) or antitumoral activity (tetranuclear platinum functionalized metallodendrimer[29] DAB(PA-tPt-Cl)$_4$ based on the polyamino G1 PPI dendrimer or sodium carboxylate generation 3.5 PAMAM, which coordinates cisplatin).[30]

The EPR technique has proved very valuable in providing unique information on the complexation ability of different dendrimers towards Cu^{2+} and Mn^{2+}. By using copper ions as spin probes, it was possible to characterize the dendrimer structure with respect to the distribution and fluidity of different interacting sites in the dendrimer interior and at the external surface.[10,18,20–25]

Following up our previous work[31,32] on the synthesis of metal mono-nuclear compounds with antiviral activity, and the dendrimer EPR characterization work by using copper complexation,[10,18,20–25] we now report the synthesis and characterization of first, second and third generations of PPI dendrimers with an ethylenediamino (EDA) core. We selected a divergent procedure[33] for the synthesis of PPI dendrimers from the EDA core, which avoided the use of metal catalysts. These PPI dendrimers with amino groups in their periphery were used as precursors for the synthesis of polysulfonate and polycarboxylate dendrimers, by means of Michael-type addition reactions.[34] These precursor modifications overcome polyamino associated toxicity, increasing dendrimer biocompatibility and improving coordination properties towards metal ions, by providing better metal chelating moieties in the periphery. We evaluated the metal complexing behavior of these polyanionic dendrimers using Cu^{2+} as a probe, characterizing specificity in the complexing pattern through UV-Vis spectrophotometry and EPR experiments at increasing Cu^{2+}/dendrimer molar ratios. This specificity allows us to prepare different transition metallodendrimers which are being evaluated as inhibitors of HIV infection at the moment.

Results and discussion

In our previous work,[31,32] we synthesized and characterized some sulfonate and carboxylate-containing N-donor ligands, and their corresponding metal (Ni, Co, Cu and Zn) complexes. These complexes inhibited HIV infection when treating both pre- and post-infected PBMC.

In order to continue evaluating this synergic behaviour of metal ions and polyanionic ligands, we were interested in the preparation of dendritic polyanionic ligands capable of coordinating metal ions both in their interior and their periphery. To achieve this objective, we synthesized PPI dendrimers which present an EDA core and polycarboxylate or polysulfonate periphery, and evaluated their metal complexing ability.

In all cases, we followed Meijer's naming system for poly(propylene imine) dendrimers: core-*dendr*-termini, which indicates the number of terminal groups in the structure.

Synthesis and characterization of precursor dendrimers

As precursor dendrimers, we designed new poly(propylene)imine (PPI) dendrimers with an EDA core. The synthesis was carried out through Vögtle's iteration.[33] In the first step, Michael-type addition of an excess of acrylonitrile to ethylenediamine, at reflux for 18 h with AcOH as a catalyst, and subsequent evaporation to dryness, yielded the tetranitrile EDA-*dendr*-$(CN)_4$ (**1**), which was used as the starting point for the iterative divergent synthesis of the rest of the polynitrile and polyamine dendrimers. The second step in the iterative route consisted of the reduction of (**1**), dissolved in THF, to the tetra-amine EDA-*dendr*-$(NH_2)_4$ (**2**) using $BH_3{\cdot}Me_2S$ in Et_2O at 60 °C, followed by methanolysis of the borane adduct. This iterative sequence was applied to obtain the second (EDA-*dendr*-$(CN)_8$ (**3**) and EDA-*dendr*-$(NH_2)_8$ (**4**)) and third generation (EDA-*dendr*-$(CN)_{16}$ (**5**) and EDA-*dendr*-$(NH_2)_{16}$ (**6**)) dendrimers.

The two-step sequence of the synthesis of these dendrimers is indicated in Scheme 1. This procedure avoided the typical use of metal catalysts for nitrile reduction which could be bound to the final product, and allowed the completion of the reduction step.

Synthesis and characterization of polyanionic dendrimers

Polyanionic dendrimers were synthesized from their precursors, by means of the method developed by Liang *et al.*[34] using Michel-type addition reactions.

The conjugate addition of polyamine dendrimers **2**, **4** and **6** to sodium vinylsulfonate in aqueous solution and ratios 1 : 8, 1 : 16 and 1 : 32, respectively, at 120 °C for 48 h led to the formation of polysulfonate dendrimers EDA-*dendr*-$(SO_3Na)_8$ (**7**, generation 1), EDA-*dendr*-$(SO_3Na)_{16}$ (**8**, generation 2) and EDA-*dendr*-$(SO_3Na)_{32}$ (**9**, generation 3), which will be renamed in this paper for simplicity as G1S, G2S and G3S, respectively. They are obtained as pure yellow solids after their purification by nanofiltration devices for 1 day with cutoff membranes of MW = 500–1000 g mol^{-1}. The proposed structures for dendrimers **7–9** are displayed in Fig. 1.

For dendrimer **7**, the ^{1}H-NMR spectrum in D_2O (Fig. 2) shows the methylene units of the ethanesulfonate fragment with two multiplets at δ = 2.95 ppm for the –CH_2S– unit and 2.81 ppm for the –NCH_2– unit on the basis of NOESY experiments, the latter overlapped with the singlet assigned to the equivalent methylene groups –$^cNCH_2CH_2N^c$–, where

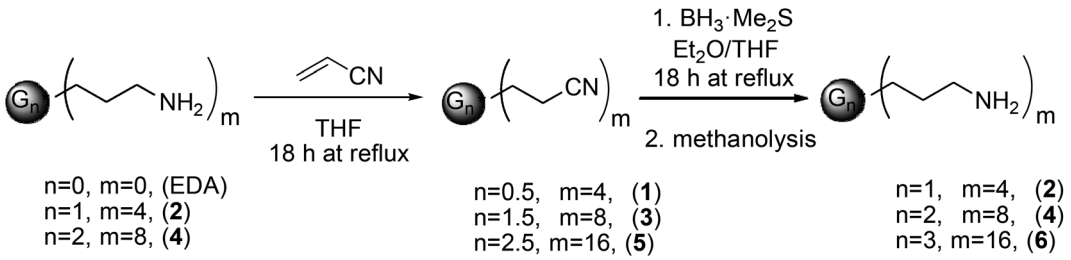

Scheme 1 Synthesis of precursor dendrimers **1–6**.

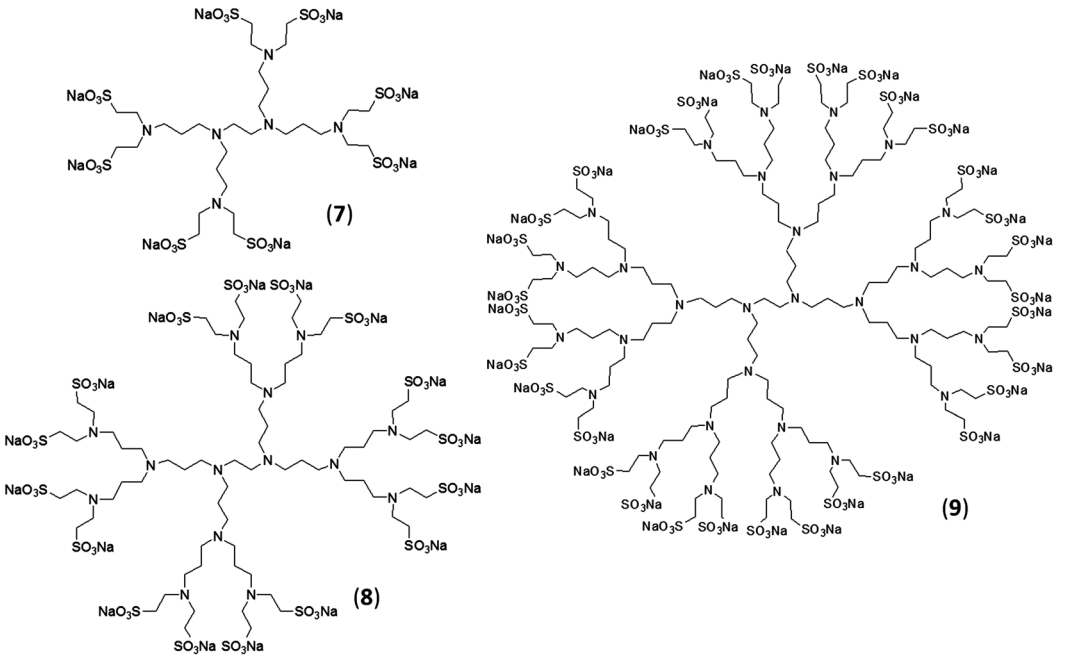

Fig. 1 Proposed structures for polysulfonate dendrimers **7**, **8** and **9**.

superscript "c" indicates the nitrogens at the core. The methylene groups of the chain $-^{c}NCH_2CH_2CH_2N-$ are observed (from the core to the periphery) as multiplets at δ = 2.40, 1.60, and 2.60 ppm.

Respecting the ^{13}C-NMR spectrum, six resonances were observed and assigned on the basis of HMQC experiments. The resonances at δ = 47.6 and 47.0 ppm are attributed to $-NCH_2-$ and $-CH_2S-$ fragments of the ethanesulfonate group in that order. The methylene groups $-^{c}NCH_2CH_2N^{c}-$ at the core appear at δ = 50.3, while those from the chain $-^{c}NCH_2CH_2CH_2N-$ appear at δ = 51.0, 22.0 and 52.8 (from the core to the periphery).

For 2 and 3 generation dendrimers **8** and **9**, the ^{1}H-NMR and ^{13}C-NMR spectra follow a similar pattern, but the signals become less resolved as the generation grows (*see the Experimental section*).

In an analogous way to the sulfonated dendrimers, and following the same synthetic route as Duijvenbode[35] *et al.* for similar carboxylate dendrimers, the addition of an excess of methyl acrylate to the polyamine dendrimers **2**, **4** and **6** at 80 °C for 18 h gave poly(methylester) dendrimers EDA-*dendr*-$(CO_2Me)_8$ (**10**), EDA-*dendr*-$(CO_2Me)_{16}$ (**12**) and EDA-*dendr*-$(CO_2Me)_{32}$ (**14**). These compounds are the precursors of polycarboxylate dendrimers EDA-*dendr*-$(CO_2Na)_8$ (**11**, generation 1), EDA-*dendr*-$(CO_2Na)_{16}$ (**13**, generation 2) and EDA-*dendr*-$(CO_2Na)_{32}$ (**15**, generation 3), which will be renamed in this paper for simplicity as G1C, G2C and G3C, respectively. The addition of aqueous sodium hydroxide to the ester precursors led to the formation of these sodium salt forms, which are soluble in water and methanol, slightly in ethanol and insoluble in organic solvents. These compounds were also purified by nanofiltration devices for 1 day with cutoff membranes of MW = 500–1000 g mol^{-1}. The proposed structures for dendrimers **11**, **13** and **15** are displayed in Fig. 3.

Poly(methylester) dendrimers **10**, **12** and **14** were characterized by NMR in $CDCl_3$. In the ^{1}H-NMR spectrum of **10** (Fig. 4), the methyl ester group CO_2Me shows a singlet at δ = 3.63 ppm, while the methylene units of the ethanecarboxylate fragment appear as two multiplets at δ = 2.73 ppm for the $-CH_2N-$ unit and 2.41 ppm for the $-CCH_2-$ unit on the basis of NOESY experiments, the latter overlapped with all the signals for $-NCH_2-$ groups, from the core and the chain. The intermediate

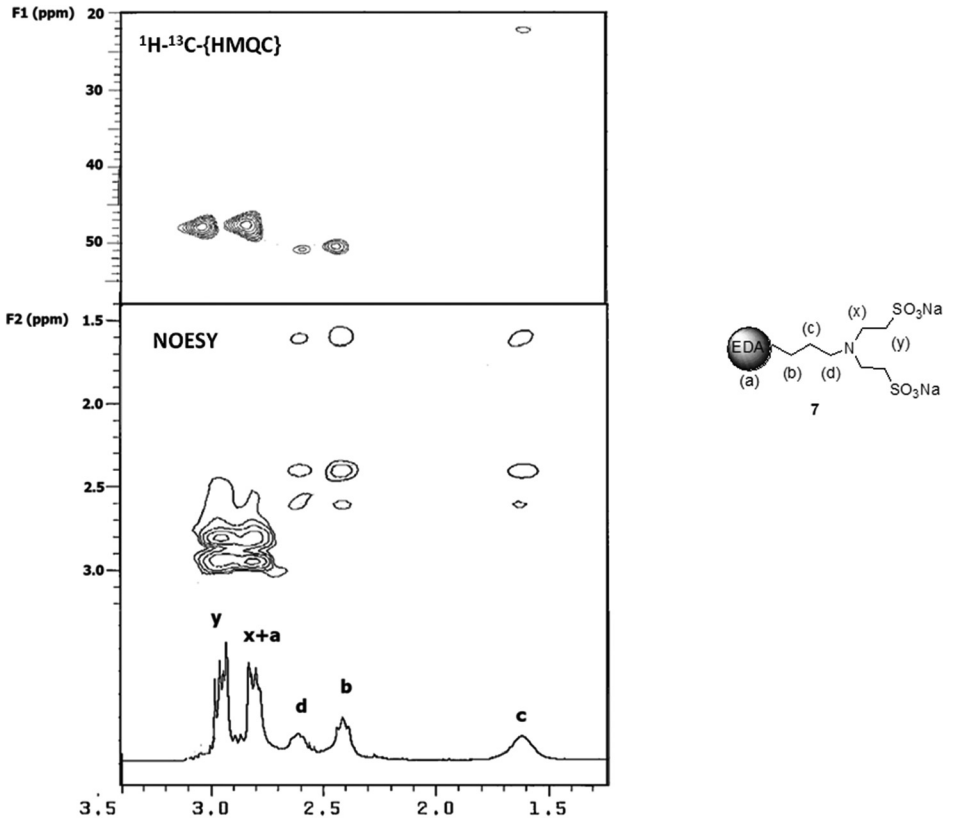

Fig. 2 ^{1}H-^{13}C-{HMQC} and NOESY spectra of polysulfonate dendrimer **7**.

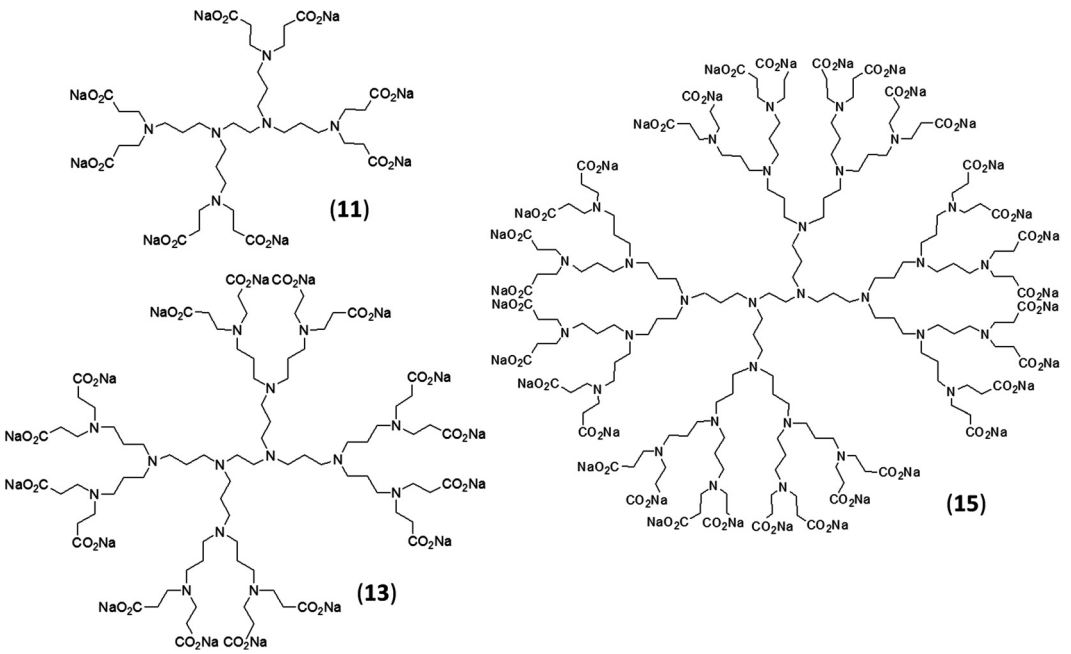

Fig. 3 Proposed structures for polycarboxylate dendrimers **11**, **13** and **15**.

methylene group of the chain –$NCH_2CH_2CH_2$N– is observed at δ = 1.52 ppm as a multiplet.

In the ^{13}C-NMR spectrum, the resonances were assigned on the basis of HMQC experiments; for the CO_2Me fragment, two resonances at δ = 173.0 and 51.5 ppm are observed, for the carbonyl and the methyl groups respectively. The resonances at δ = 49.1 and 32.4 ppm are attributed to –NCH_2– and –CH_2C– fragments of the ethanecarboxylate group in that order, and

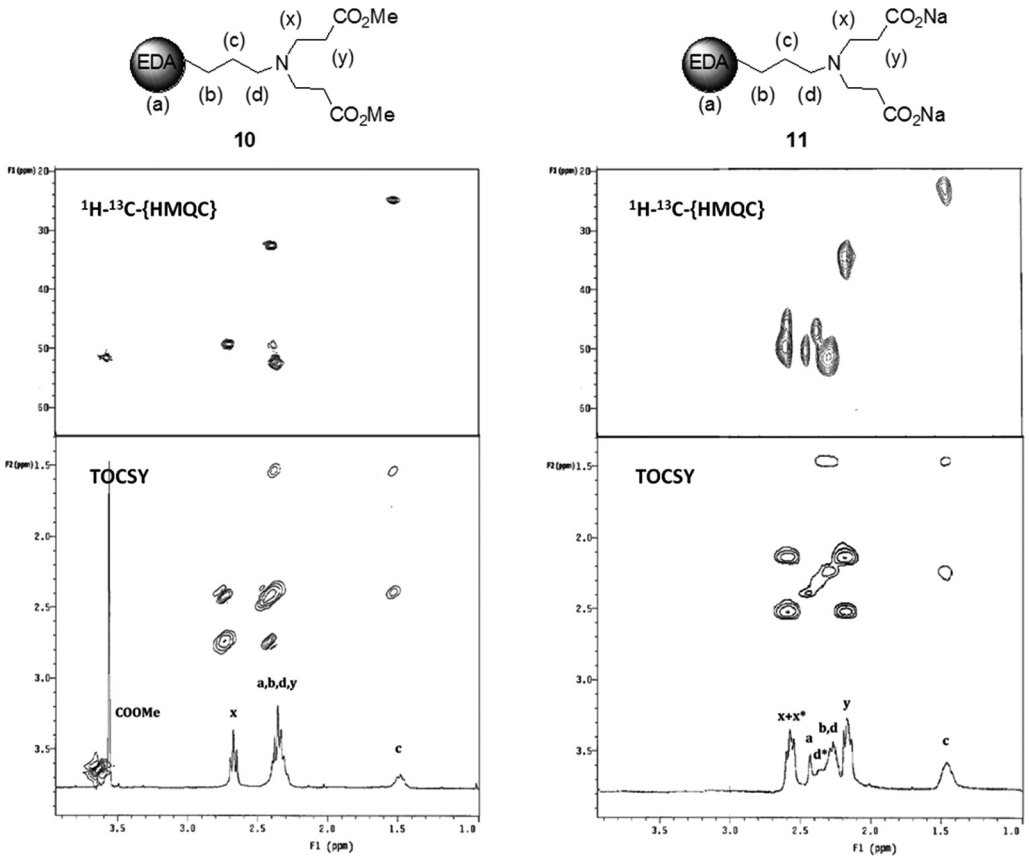

Fig. 4 ^{1}H-^{13}C-{HMQC} and TOCSY spectra of polycarboxylate dendrimers **10** and **11**. Signals with * are indicative of a partial N-protonation process.

the methylene groups –NCH_2– are observed at δ = 52.5, 52.4 and 51.8 ppm.

The precursor dendrimers **12** and **14** show similar NMR data to those of **10** (*see the Experimental section*).

Polycarboxylate dendrimers **11**, **13** and **15** were characterized by NMR experiments in D_2O. In the ^{1}H-NMR spectrum of **11** (Fig. 4), the methylene units of the ethanecarboxylate fragment appear as two multiplets at δ = 2.56 ppm for the –NCH_2– unit and 2.18 ppm for the –CH_2C– unit on the basis of NOESY experiments. Also, at δ = 2.42 ppm a singlet is observed for the equivalent methylene groups –NCH_2CH_2N–, while the other methylene groups from the chain –$^{c}NCH_2CH_2CH_2N$– appear (from the core to the periphery) at δ = 2.32, 1.45 and 2.26 ppm. The small multiplets, indicated with an asterisk, at δ = 2.55 (x*) and 2.35 (d*) ppm are indicative of partial protonation of the peripheral amino groups at the measurement pH, which provokes the slight displacement of the methylene groups bound to this N atom.

In the ^{13}C-NMR spectrum of **11**, the resonances were assigned on the basis of HMQC experiments; for the CO_2Na fragment, the carbonyl group shows a resonance at δ = 181.5. The resonances at δ = 49.8 and 37.5 ppm are attributed to –NCH_2– and –CH_2C– fragments of the ethanecarboxylate group in that order. The –NCH_2CH_2N– groups appear at δ = 49.9, while the methylene groups from the chain –$^{c}NCH_2CH_2CH_2N$– at (from the core to the periphery) δ = 53.7, 24.0 and 53.7 ppm. The small signals at δ = 36.4 (y*), 46.0 (x*) and 46.5 (d*) ppm arise from the partial N protonation, which implies a partial zwitter-ionic form of the carboxylate group, as indicated by the small signal at δ = 180.3 ppm (COOH*).

For 2 and 3 generation dendrimers **13** and **15**, the ^{1}H-NMR and ^{13}C-NMR spectra follow a similar pattern, but the signals become less resolved as the generation grows (*see the Experimental section*).

Potentiometric titrations of polyanionic dendrimers

These sulfonate and carboxylate PPI dendrimers can be considered as the higher generations of the ligands previously synthesized by our group,[31,32] whose complexing power has been demonstrated. They present not only multiple coordination sites at the periphery, but also a functional interior of tertiary amines, which make them potential complexing agents.[6]

We studied the acid–base properties of these modified PPI dendrimers in order to understand their complexing power. As previously demonstrated for carboxylate PPI dendrimers with the DAB core,[35] the interpretation of the titration data can be based on a modified Ising model, which is extended to a branched polyelectrolyte with a combination of two types of ionizable groups. The protonation behaviour of the dendrimers depending on the pH of the medium was studied *via* potentiometric titration in pure distilled water without ionic strength, and the experimental values of pK_a calculation were

carried out using the method of the second derivative[36] (Fig. 5). A theoretical calculation of the pK_a values of each group and a simulated distribution of macrospecies, determined by the Marvin, Calculator Plugin and Chemical Terms Demo,[37] are depicted in the ESI,† for a better understanding of the experimental results.

In previous studies,[32] the titration curve of the sulfonated ligand (or 0 generation dendrimer) showed two pK_a values with a pronounced difference between them (4.63 and 9.12), assigned to the two acidic dissociation constants of the ammonium groups, as the protonation of sulfonated groups occurs at very low pH. For the analogous carboxylate ligand, we also observed two pK_a values (5.01 and 8.09), the first of them as a broad peak which included other protonation processes associated with the carboxylate groups.

We detected that this behaviour can be extended to the rest of the generations. For the sulfonate dendrimer of generation 1 (**7**), the titration curve displays two clearly different pK_a values (4.57 and 8.40), which we assign to the acidic dissociation constants of the two types of ammonium groups. This result agrees with the theoretical calculation, which indicates that at physiological pH the predominant macrospecies presents 4 nitrogens protonated, from both the core and the first layer, and all sulfonate groups in their ionic form. For the carboxylate dendrimer of generation 1 (**11**), again we observed two pK_a values (5.72 and 8.37), the first of them appearing more complex as it includes the protonation processes for the carboxylate groups. This way, the last parts of the titration curves overlap. According to the theoretical values, the first includes the core nitrogens and all carboxylate acid–base processes, while the second encompasses the protonation of nitrogens in the first layer. In this case, at physiological pH the predominant macrospecies presents all the nitrogens in the first layer protonated, while those from the core and the carboxylate groups are deprotonated.

Metal complexation study

These polyanionic dendrimers are candidates for complexing metal ions in their structure, both in the polyamino core and skeleton, and in the polyanionic surface. The metal complexing ability of the dendrimers was studied by using Cu^{2+} as a probe. We performed the Cu^{2+} titration of the different dendrimers, and followed it by UV-Vis and EPR spectroscopy.

UV-Vis characterization. We performed the copper titration of dendrimer samples at a concentration of 0.1 mM, in distilled water. We evaluated three different points of coordination of the dendrimer structure, which correspond to different dendrimer : metal ratios (for generation 1, ratio D : M = 1 : 1, 1 : 3 and 1 : 5; for generation 2, ratio D : M = 1 : 1, 1 : 5 and 1 : 9; for generation 3, ratio D : M = 1 : 1, 1 : 9 and 1 : 17). The results are described in Table 1.

Copper titration of G1C (**11**) followed by UV-Vis spectrophotometry is shown in Fig. 6. After the addition of the first equivalent of copper, an LMCT band around 300 nm and a d–d transition band around 660 nm appear. According to our previous results, these bands are indicative of coordination through the ethylenediamine group in the core of the dendrimer.[32] The following two equivalents give rise to a shoulder at 260 nm, related to the coordination of carboxylate groups to the metal ion, and an increase of the band around 300 nm, probably because more nitrogen atoms are coordinated. The d–d transition band is displaced to higher wavelengths, as there is an increase in the number of oxygens coordinated to the metal ion, with a possible octahedral CuN_2O_4 or square-

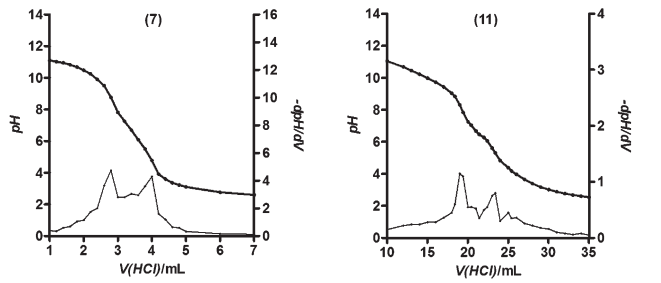

Fig. 5 Experimental titration curves of first generation dendrimers **7** and **11**.

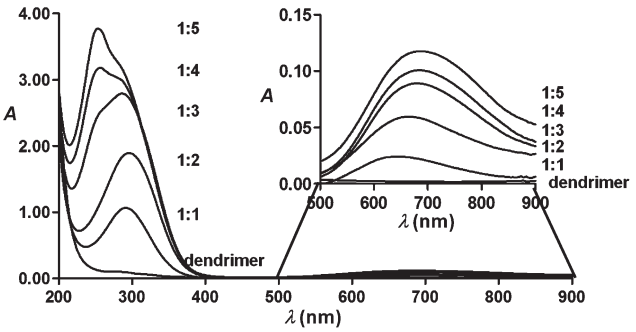

Fig. 6 Copper titration of G1C (**11**) followed by UV-Vis spectrophotometry.

Table 1 UV-Vis absorption (maximum values) of the metallodendrimers. LMCT–MLCT (200–300 nm), $^2E_g \rightarrow {}^2T_{2g}$ (600–900 nm). Reference values for the d–d transition band: "CuO_6" (hexaaquocomplex, 794 nm), "CuN_6" ($[Cu(1\text{-allylimidazole})_6]^{2+}$, 578 nm). "s" stands for "shoulder"

Dendrimer	1st point		2nd point		3rd point	
G1S (**7**)	(1 : 1)	295/663	(1 : 3)	295/709	(1 : 5)	295/741
G2S (**8**)	(1 : 1)	295/657	(1 : 5)	295/678	(1 : 9)	295/753
G3S (**9**)	(1 : 1)	298/652	(1 : 9)	298s/694	(1 : 17)	298s/759
G1C (**11**)	(1 : 1)	298/658	(1 : 3)	258s/298/674	(1 : 5)	250/298s/701
G2C (**13**)	(1 : 1)	288/666	(1 : 5)	254s/286/684	(1 : 9)	246/298s/690
G3C (**15**)	(1 : 1)	279/655	(1 : 9)	257/280s/675	(1 : 17)	252/280s/688

planar $CuNO_3$ coordination, depending on the flexibility of the branches.

Finally, with the last two equivalents, the band at 280 nm remains constant, due to the saturation of the nitrogen centers, while the band at 260 nm continues growing, and the d–d transition band is again displaced, to a square planar coordination of $CuNO_3$, which may include a water molecule.

The higher generations of the carboxylate dendrimers follow a similar pattern, in their respective coordination points (see ESI†). However, at the highest copper concentrations tested, they show a different behavior from the first generation dendrimer. Both of them show a continuous increase of the LMCT band, until reaching 11 (**13**) or 25 (**15**) copper equivalents. In addition, the d–d band maximum suffers a shift to lower wavelength, especially clear in **15**. All of this evidence points to a relocation of copper atoms between the periphery and the interior of the dendrimer, increasing the number of coordinated internal nitrogens, which also correspond to the appearance of some turbidity in the solution indicative of a progressive decrease in the solubility of the compound in water.

As we had previously described,[32] in the case of sulfonate complexes, the LMCT band is of lower intensity, with respect to that of carboxylate complexes, indicating a weaker interaction with nitrogens, in favor of a stronger coordination with the sulfonate oxygens. This way, in carboxylate complexes this LMCT band is more intense, demonstrating a preferential N coordination to the carboxylate oxygens. This behavior is again found in copper titration of polyanionic dendrimers.

Copper titration of G1S (**7**) followed by UV-Vis spectrophotometry is shown in Fig. 7. In this case, after the addition of the first equivalent of copper, an LMCT band around 295 nm and a d–d transition band around 660 nm appear, due to the coordination in the dendrimer core. The following equivalents show a little increase in the intensity of the LMCT, and a progressive displacement of the d–d transition band to higher wavelengths, as there is an increase in the number of oxygens coordinated to the metal ion. In this case, this displacement is due to the stronger coordination to the sulfonate oxygens, compared to the carboxylate ones. Again, the higher generations of the sulfonate dendrimer follow a similar pattern, in their respective coordination points.

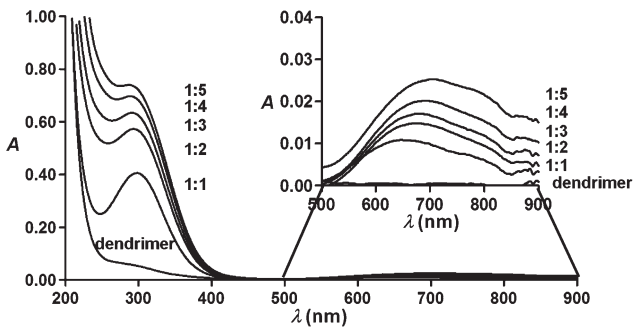

Fig. 7 Copper titration of G1S (**7**) followed by UV-Vis spectrophotometry.

All of this evidence is in agreement with the EPR results (*vide infra*).

EPR characterization. Characterization of interacting ability, dynamics and structure of PPI dendrimers with the EDA core and external surface functionalization with sulfonate (**7**, **8** and **9**) and carboxylate (**11**, **13** and **15**) groups was carried out by means of a computer aided electron paramagnetic resonance (EPR) analysis of the spectra of Cu^{2+} complexes, both at room (298 K) and low (150 K) temperatures, using increasing Cu^{2+} concentrations.

This analysis provided detailed information about the dendrimer interacting properties, in order to use these compounds and their metal complexes for future biomedical purposes.

EPR spectra were analyzed using the programs NLSL, by Budil and Freed,[38] and the SimFonia, by Bruker (version 1.25). Also the program CU3XP, kindly provided by Prof. Romanelli, University of Florence (Italy), was used for comparison purposes. To interpret the EPR parameters, we mainly refer to previous literature where the EPR analysis was performed by means of a similar approach.[10,18,20,21]

Dendrimers were dissolved at a concentration of 0.1 M in surface external groups, giving dendrimer concentrations of 12.5 mM (generation 1, 8 surface groups), 6.25 mM (generation 2, 16 surface groups) and 3.125 mM (generation 3, 32 surface groups), while the Cu^{2+} concentration was increased from 0.0025 to 0.25 M.

In order to check our previous results through UV-Vis spectrophotometry, on the specificity of the first copper equivalent into the dendritic core, we started our EPR analysis from the smallest Cu^{2+} concentration (0.0025 M). Copper concentrations lower than 0.0025 M provided a too low signal-to-noise ratio which did not allow us to perform a correct and reproducible spectral analysis.

At a Cu^{II} concentration of 0.0025 M, the room temperature spectra of GnC dendrimers are constituted by two components (Fig. 8a).

For G1C (**11**), the spectra at both room (Fig. 8b) and low (Fig. 8c) temperatures may be computed by a single component (termed *Signal I*) indicative of strong coordination with nitrogen sites ($Cu–N_2O_2$ or $Cu–N_3O$), probably involving carboxylate ligands in the equatorial and/or in the axial positions. This component decreases in relative intensity, especially from G1 to G2, but also from G2 to G3 (Fig. 9a), which is related to the dendrimer structural properties. For G1C, at Cu^{2+} concentrations up to 0.01 M, the line shape does not change while the intensity proportionally increases (Fig. S1-ESI† and Fig. 9a). Then, from 0.015 M, a second spectral component starts increasing while the first component does not increase anymore and the overall intensity of the EPR spectrum starts poorly increasing (Fig. 9a). The second component (termed *Signal II*) is a broad poorly-resolved line, corresponding to an interaction mostly involving the external carboxylate groups and water molecules. These results are nicely in line with the interaction of Cu with the internal core at a 1 : 1 ratio between Cu^{II} and the dendrimer balls: since the G1C concentration in

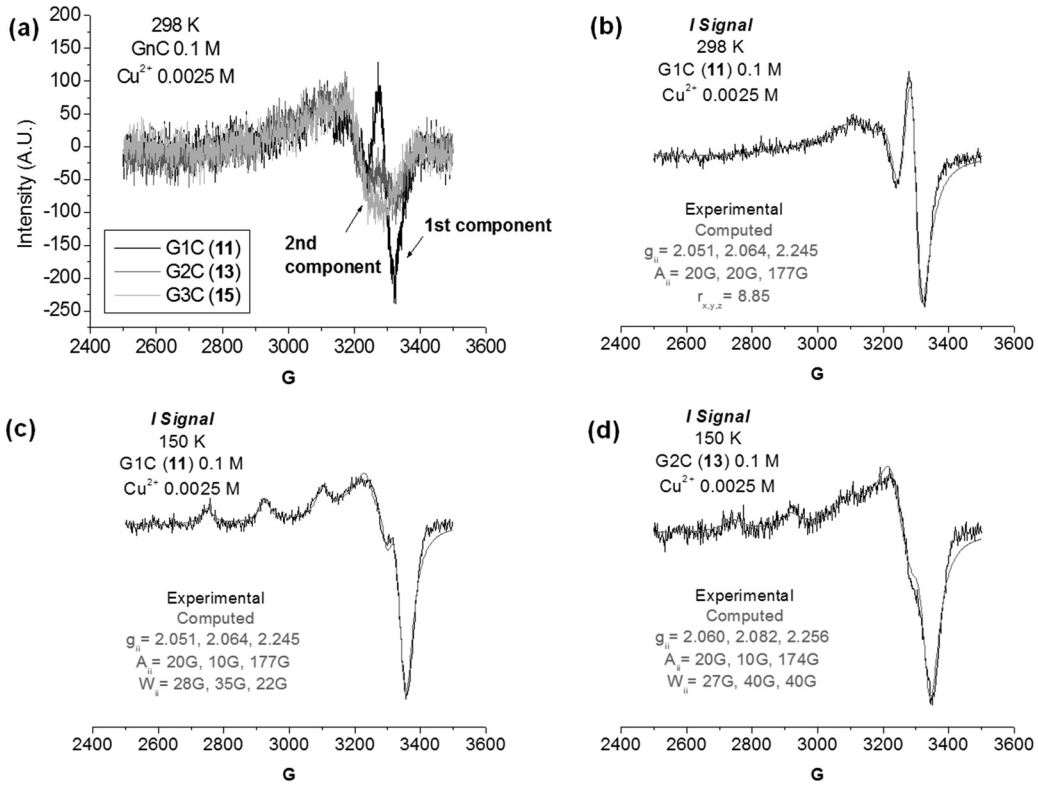

Fig. 8 (a) Experimental EPR spectra of carboxylate dendrimers at 298 K, at a copper concentration of 0.0025 M. (b)–(d) Experimental (black) and computed (gray) EPR spectra of **11** at 298 K (b) and 150 K (c), and of **13** at 150 K (d) at a copper concentration of 0.0025 M.

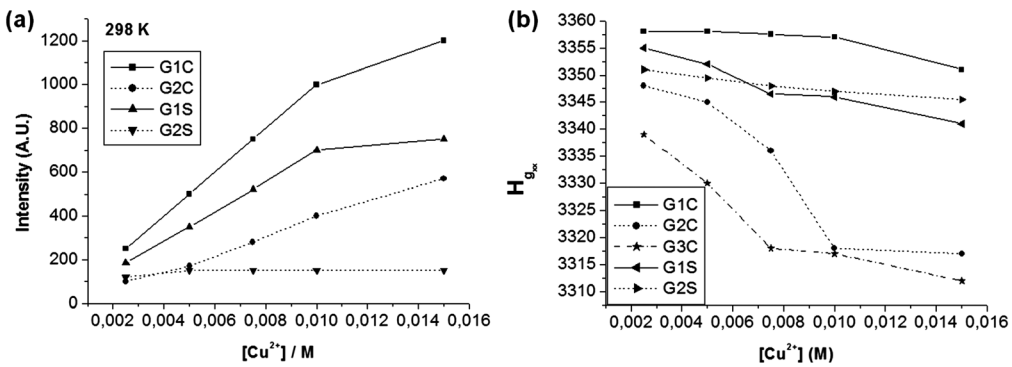

Fig. 9 Variation of (a) the intensity of the room temperature spectra, and (b) the high field minimum of the low temperature EPR spectra of the different dendrimers, when increasing copper concentration.

dendrimer balls is 0.0125 M, the spectrum does not change up to about this Cu concentration. After saturation of the internal dendrimer sites at the core position, only the external surface groups are available for copper complexation, and strong spin–spin interactions occur between close ions leading to formation of EPR silent Cu^{II} dimers.

For G2C (**13**), a surprisingly high relative concentration of the second component (about 40%, as obtained after spectral subtraction) already present at $[Cu^{2+}]$ = 0.0025 M (Fig. 8a) was found. From G1 to G2, the first component almost disappeared, while the second component remained unchanged. This decrease in the EPR intensity of the first component may be explained by a strong spin–spin exchange between ions close to each other internally in the dendrimer structure: for G2C with respect to G1C, more nitrogen sites are available for copper binding, without causing a strong repulsion between the charged ions. In line with this hypothesis, it was found that an increase of copper concentration caused a non-linear growth of the intensity of the first component (Fig. S1-ESI†), which stopped at about 0.0075 M (1.2 eq.) and it was no more distinguishable at 0.01 M (1.6 eq.), in line with a saturation of the dendrimer core. Also the overall intensity of the spectra did not increase linearly with the copper concentration, as shown in Fig. 9a, due to strong spin–spin interactions.

Moreover, although computation of G1C spectra indicated a coordination with 2–3 nitrogen sites (1–2 Cu atoms in the core), UV-Vis analysis pointed to a 1 : 1 complexation, supported by a high repulsion between copper ions in close space.

A further explanation about the differences between G1 and G2 spectra arises from the structure of the dendrimers. For G1C, first, the core is an open space where copper ions are free to go far away from each other; second, although there are less nitrogen sites available, they belong to more flexible branches (with respect to G2) which approach the ions giving rise to a less distorted square planar coordination with them.

Indeed, it was found that, at $[Cu^{2+}]$ = 0.0025 M, the room temperature first component for G2C is less mobile than the same component of G1C, but it could also be seen in Fig. 8 that the low temperature spectrum of G2C may be computed (Fig. 8d) as a single component characterized by lower A_{zz} and higher g_{zz} values with respect to the low temperature spectrum of G1C (Fig. 8c) at the same copper concentration. So, at low temperature the second component for G2C is either masked by the first one or it disappears due to salt separation, while the first component revealed a broadening due to spin–spin interactions and parameters which indicate a weaker (or simply more distorted) coordination with nitrogen sites with respect to G1C.

The situation for G3C (**15**) is in line with the trend found from G1C to G2C. In this case, the available space in the core is wider and more nitrogen sites are also available; in agreement with this finding, at $[Cu^{2+}]$ = 0.0025 M, the percentage of the second component was higher than 80%, while the first component largely disappeared due to spin–spin interactions, and the line shape poorly changed by increasing Cu^{2+} concentration. The intensity of the spectrum linearly increased up to $[Cu^{2+}]$ = 0.0075 M (2.4 eq.) and then remained unchanged until 0.01 M (3.2 eq.), indicating that more than one copper ion is entering into the dendrimer cavities to interact with the N sites.

For a better understanding of the dendrimer behaviour, it is interesting to monitor the variation of the high field minimum (called Hg_{xx}) of the low temperature spectra in the Cu^{II} concentration range 0.0025–0.015 M (Fig. 9b), which follows the trend of the g_{xx} value of the main component (an increase in g_{xx}, that is, a decrease in Hg_{xx}, reflects a smaller or weaker coordination with the nitrogen sites). For carboxylate dendrimers, Fig. 9 clearly shows that, at the same copper concentration, the Hg_{xx} sequence is G1 > G2 > G3, and, interestingly, Hg_{xx} starts decreasing at different copper concentrations for the three dendrimers, depending on the value at which a Cu^{2+} : dendrimer molar ratio = 1 : 1 is attained. These results are in line with the saturation of the nitrogen core at a ratio of 1 : 1.

Moreover, these Hg_{xx} values, together with all the magnetic parameters extracted from computation, also reflect the different interacting abilities of the dendrimers at different generations, due to different (a) void space, (b) branch flexibility, and (c) nitrogen site availability in the dendrimer core. Of course these interactions are possible because of a relatively weak interaction of Cu^{II} with the carboxylate groups. Indeed, only after the nitrogen sites are almost totally occupied, the carboxylate groups become the only sites involved in the complexation together with solvent molecules.

The evidence of the role played by a stronger interacting negatively charged surface was clarified by analyzing the EPR spectra of the sulfonate decorated dendrimers. The complexation ability of these dendrimers was revealed by comparing their spectra with those of the carboxylate dendrimers (Fig. S2-ESI†), mainly on the basis of the plots shown in Fig. 9.

At $[Cu^{2+}]$ = 0.0025 M (Fig. S2a-ESI†), G1C gives a stronger interaction with the nitrogen sites than G1S. This is evident because the last hyperfine line shifted to left from G1C to G1S, which corresponds to a decrease in Hg_{xx} (Fig. 9b). From G1S to G2S the variation is similar but smaller than the variation from G1C to G2C described above. Both these findings are in line with a stronger complexation of Cu^{II} with SO_3^- with respect to CO_2^-. But, also interestingly, from the carboxylate to the sulfonate dendrimers, as well as from generation 1 to generation 2, the spectra show a decrease in intensity which may be correlated to the formation of dimeric copper complexes (Fig. 9a).

Initially, we expected a linear growth of the spectral intensity with the increase in Cu^{II} concentration, as such as we expected an equivalence of intensity at the same Cu^{II} concentration for the different dendrimers. However, this unexpected decrease in intensity from G1 to G2, as such as from carboxylate to sulfonate dendrimers, nicely indicated the formation of dimeric (or more than two) copper complexes. So, for G2S the almost unchanged intensity by increasing the Cu^{II} concentration is due to the fact that, after and while coordinating the internal sites, the ions also interact with the close sulfonate groups by forming dimeric species.

The spectra of G1S with Cu^{2+} concentration in the range 0.005–0.015 M are constituted by two components which change their relative percentages with the increase in copper concentration. Fig. 10a shows the variation over Cu^{2+} concentration of the relative percentage of the so-called *I Signal*, the component which is under slow motion conditions at room temperature. This signal significantly decreases in relative intensity by increasing $[Cu^{2+}]$, reaching a plateau at 12.5 mM (1 eq. of copper). As indicated by the slow motion at room temperature and by the magnetic parameters obtained from computation (Fig. 10b), the slow component arises from copper ions trapped at the internal dendrimer layer and coordinating with two nitrogen sites and 2 oxygen sites (CuN_2O_2) belonging to the sulfonate groups or water molecules. The decrease in intensity corresponds to the saturation of these sites and the consequent pushing of the extra ions to the external surface, where, on the basis of the magnetic parameters (Fig. 10c), copper is coordinated by surface oxygen sites, but, probably, it still retains one nitrogen site (*II Signal*).

Our results are in close agreement with the studies of G_0 unmodified PAMAM dendrimers with the EDA core with one copper equivalent,[39] where the authors use density functional theory (DFT) calculations and EPR studies to demonstrate that at pH = 7.8, it forms a chelating complex with two tertiary amine sites with or without two amide oxygen sites. Moreover,

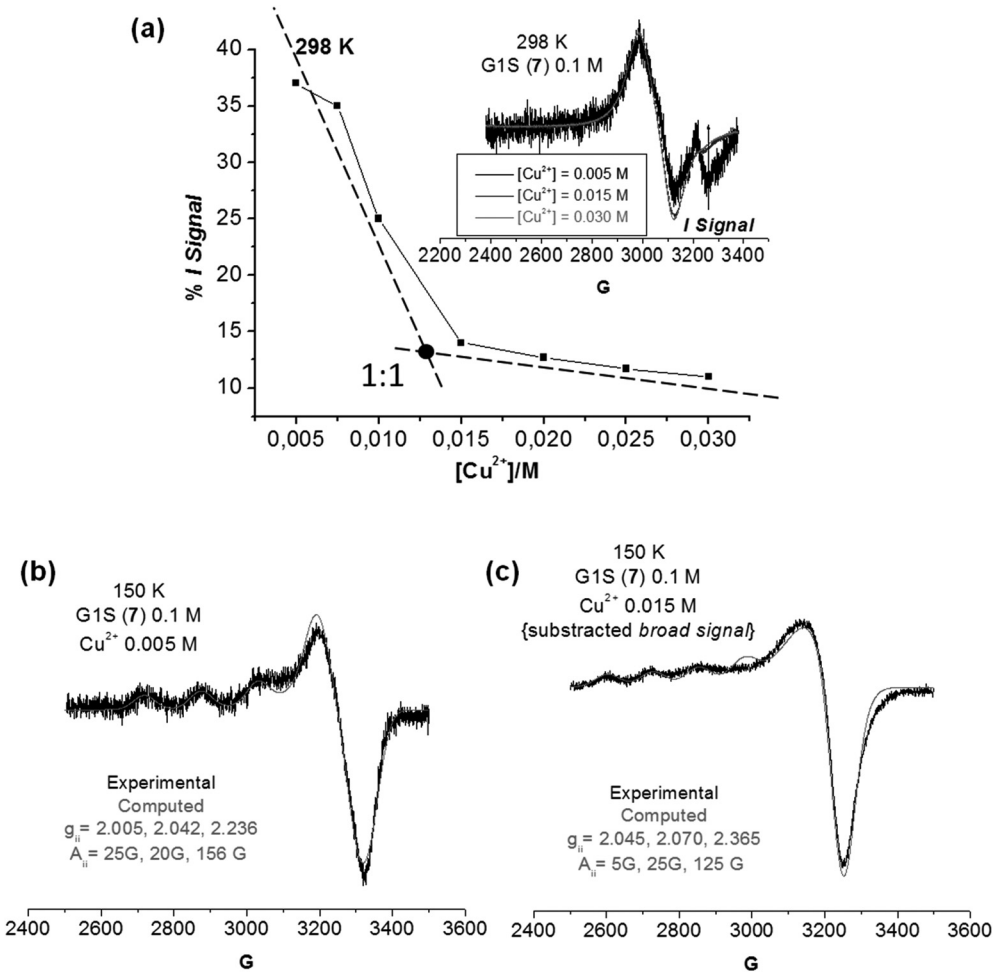

Fig. 10 (a) In the inset: experimental EPR spectra at room temperature of copper titration of G1S (**7**). In the plot: decrease in the % slow motion I signal at room temperature, when increasing copper concentration. (b)–(c) Experimental and computed EPR spectra of G1S (**7**) at 150 K at a copper concentration of 5 mM (1 : 0.4, (b)) and 15 mM (1 : 1.2, (c)).

they show that Cu^{II} or Zn^{II} chelation of the two tertiary amines in a G_4 unmodified PPI dendrimer with the diaminobutane (DAB) core is less likely due to the larger ring size at the chelating sites, which avoids the production of metallic nanoparticles.[40]

By further increasing the copper concentration, the spectra in the range 0.02–0.15 M mostly show one or two components (termed *II Signal* and *III Signal*) (Fig. S3-ESI†) which indicate the location of the ions at the external dendrimer layers and surface. For instance, the spectrum for G3C (**15**) at a Cu^{2+} concentration of 0.025 M (8 eq.) is a single component spectrum, indicated as "*II Signal*" which is computed, both at room and low temperatures, as shown in Fig. S4-ESI† with the magnetic parameters g_{ii} = 2.012, 2.090, 2.238; A_{ii} = 5 G, 5 G, 170 G. These parameters suggest a square planar coordination for $CuNO_3$. This is in agreement with the results from our previous study with carbosilane dendrimers.[41] Therefore, the Cu ions interact with the nitrogen and the COO^- sites of the external ligand groups and one water molecule. In line with this result, the ions show slow motion conditions (τ = 3 ns) at room temperature, because they are bound with the external ligands. However, at Cu^{2+} concentration 0.05 M, the G3C spectrum is mainly constituted by the same *II Signal*, that is, the same magnetic parameters, but most of the ions (60%) are more mobile (correlation time for motion = 0.1 ns instead of 3 ns; see Fig. S5-ESI†).

For G1C at $[Cu^{2+}]$ = 0.025 M, the spectrum shows two 1 : 1 components (Fig. S5-ESI†); one of them is the *II Signal*, while the other one was computed with the magnetic parameters g_{ii} = 2.031, 2.090, 2.246; A_{ii} = 15 G, 5 G, 164 G, which indicate a weaker or more distorted coordination with the nitrogen atom with respect to G3C. In this case, the increase in copper concentration up to 0.05 M produces an interesting effect, that is, a line narrowing due to Heisenberg exchange interaction among colliding ions.

A similar situation was found for G2C (**13**): at $[Cu^{2+}]$ = 0.05 M (8 eq.), a narrower not resolved signal is present, which disappears at 0.075 M (12 eq.). To help understand the origin of this signal, we have to consider the absolute intensity of these spectra: we noted a significant decrease in intensity from

0.05 M to 0.075 M, as shown in Fig. S3-ESI† (of course we expected an opposite behaviour). Therefore, the vicinal ligands at the dendrimer surface are progressively occupied by Cu^{2+} ions leading to strong spin–spin interactions which first give rise to a line broadening, then to exchange narrowing (measured by the exchange frequency Wex, added in the computation), and, finally, to the spectrum disappearance. This effect also justifies the increased mobility of the G1C and G3C complexes at room temperature discussed above (the *"resolved 4-lines Signal"* in Fig. S5*†). In line with this finding, the low temperature spectra did not change in the two cases (*II Signal* and *resolved 4-lines Signal*), but they also showed a narrowed single line arising from the strong spin–spin interactions.

At the highest copper concentrations, a further signal was identified in the room temperature spectra, termed *III Signal*, which is the same for all generations. At low temperature, as indicated with arrows in Fig. S3-ESI,† this *III signal* originates from two different signals, termed *III Signal* (H_2O) and *III Signal* (CO_2^- hydr.) both arising from a CuO_4 coordination (computations shown in Fig. S6-ESI†). At room temperature we cannot distinguish between water and COO^- groups coordinating the copper ions, because the anisotropies are averaged.

Further discussion is needed for comparing the spectra at different generations at Cu^{2+} concentrations of 0.075–0.15 M. At 0.075 M and room *T*, for G1C, the spectrum is the superposition of the *spin–spin narrowed II Signal* and the *III Signal* (we cannot exclude that some *resolved 4-lines signal* is also present, but its relative intensity is too low to be recognized); for G2C the spectrum is composed of the *II Signal* and the *resolved 4-lines Signal*; finally, for G3C, the spectrum is mainly composed of the *resolved 4-lines Signal* and the *III Signal*. Also, we noted that the spectral intensity decreases with the increase in generation. These results are well explained on the basis of the dendrimer structure, as follows. The *III Signal* is not present at this stage for the G2, but it appears at a Cu^{2+} concentration of 0.1 M, while the *II signal* still contributes up to 0.15 M. G2C has an intermediate situation for two opposite trends: by increasing generation the internal space and the number of ligands per macromolecule increase, while the branches flexibility decreases. The increase in the internal space and the number of branches per dendrimer favours the $CuNO_3$ (copper ions with 1 nitrogen and 3 oxygen sites) coordination (*II Signal*), while an increased constraint of the branches favours the CuO_4 coordination (*III Signal*). So, for G2C the increase in the internal space and the number of branches prevails on the constraint and the *II Signal* survives up to a Cu^{2+} concentration of 0.15 M. In contrast, for G3C, the constraint prevails and the *III Signal* becomes favoured. Correspondingly the EPR intensity decreases since the complexed ions are forced to remain in the dendrimer cavities and collisions in a restricted space lead to spin annulling. Finally, for G1C, the small size and the open and flexible structure helps the complexed ions to dynamically approach each other and the *spin–spin narrowed II Signal* significantly contributes, but the open structure mainly favours the ions to seat outside and generates the *III Signal*. All these results are reflected in the low temperature spectra, but it is noteworthy that the low temperature spectrum of G3C at a Cu^{2+} concentration of 0.075 M recovers intensity and it is similar to the ones at the lower concentrations. This is because at low temperature the ions cannot move inside the dendrimer cavities. Therefore, Heisenberg spin–spin interactions are avoided and the *II Signal* is recovered.

The EPR spectra at the higher Cu^{II} concentrations for sulfonate dendrimers are shown in Fig. S7-ESI† (298 K (left) and 150 K (right), for G1S (**7**), G2S (**8**), and G3S (**9**), at different Cu^{2+} concentrations). These spectra present similar components as described for the carboxylate dendrimers.

At room temperature, the spectra only show the two components, corresponding to the *II Signal* and the *III Signal*. With respect to the carboxylate systems, we note for the sulfonate systems a much higher prevalence of the *III Signal* with respect to the *II Signal* and the absence of both the *spin–spin narrowed* and the *4-lines resolved II Signals*. Furthermore, the *III Signal* is the same for both systems, but the *II Signal*, obtained after subtracting the *III Signal*, revealed similar features to those found for carboxylate dendrimers, but the magnetic and mobility parameters were different, as shown in Fig. 11 for G2S at a Cu^{2+} concentration of 0.025 M (4 eq.). All these findings are in line with a weaker interaction of Cu^{II} with the nitrogen site and a stronger interaction with the oxygen (SO_3^-) groups with respect to the interactions measured by EPR for carboxylate systems.

In line with the results described for carboxylate dendrimers, in the sulfonate case too, G2S (**8**) shows an increased relative amount of *II Signal* with respect to the *III Signal* because the increase in internal space and the number of branches prevails on the constraint, while for G3S (**9**) the branches constraint prevails and, in this case, the ions are almost prevented from reaching the nitrogen sites (only 10% of ions achieve this goal).

At low temperature, the *II Signal* was computed with the same magnetic parameters found for the computation of the *II Signal* at room temperature (see Fig. 11), but all the spectra at the lowest concentrations (0.025 and 0.05 M) show a small, but quantifiable (about 15% at 0.025 M) contribution of a signal which is the only one contributing to the spectrum recorded at a Cu^{2+} concentration of 0.05 M for G2S. In this case, the spectrum, indicated as the *II′ Signal*, was computed as shown in Fig. 12. The parameters indicate a strong interaction with one nitrogen site in a square planar structure. We hypothesize that the freezing separates the neutral Cu^{II}-G2S salt, and only the small fraction of dendrimers which have these internalized ions remains to contribute to the EPR signal. According to this hypothesis, the spectrum intensity is much lower than the intensities of the spectra recorded at the same Cu^{II} concentration for the G1 and G3 dendrimers.

Also in line with the stronger interaction with the SO_3^- groups with respect to the CO_2^- groups, the *III Signal* at low temperature mainly originated from the hydrated ligands and only at the highest Cu^{II} concentrations the *III Signal*(H_2O) starts prevailing. However, again in line with the structural

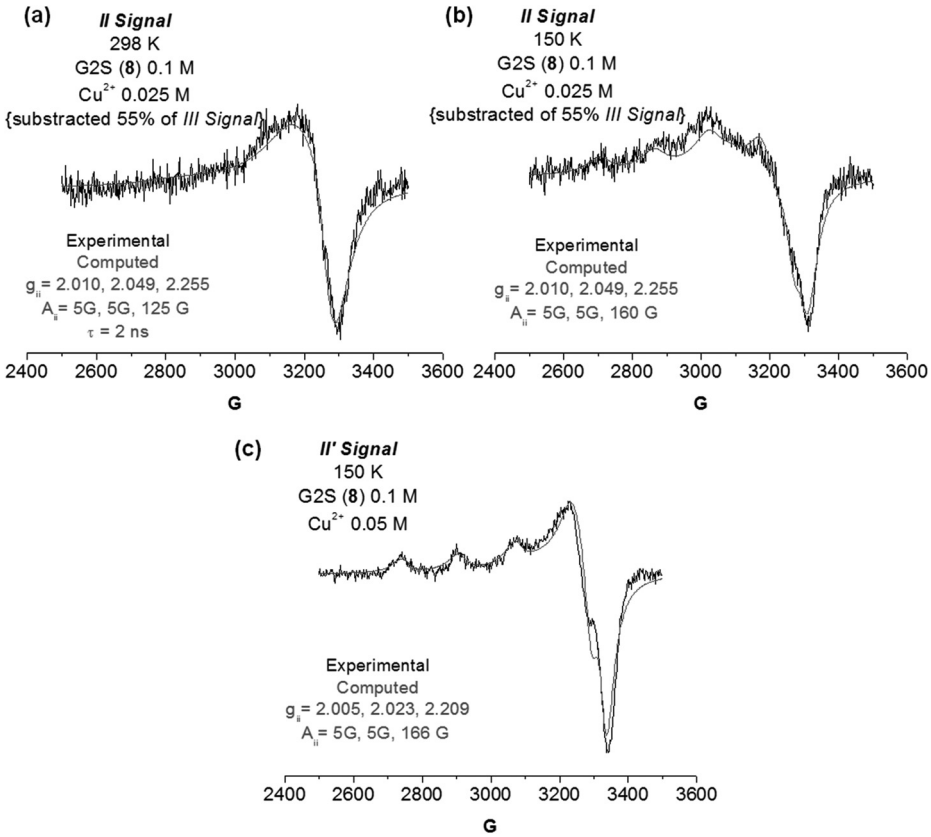

Fig. 11 Experimental (150 K, black) and computed (grey) EPR spectra of sulfonate dendrimer G2S (**8**), showing the differences between *II Signal* and *II' Signal*.

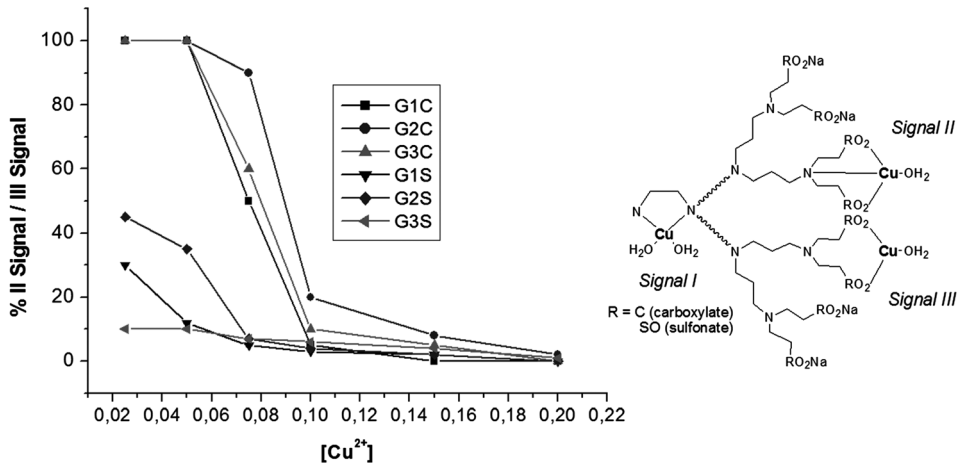

Fig. 12 % of *II Signal*/*III Signal* for the different dendrimers at increasing copper concentration.

effects discussed above, for G2S the *III Signal*(H_2O) only appears at Cu^{2+} concentrations higher than 0.1 M, while for G1 and G3 it starts appearing at the lower concentrations.

For summarizing the relative contributions of the *II and III Signals* discussed above for all the systems, the graph in Fig. 12 reports the variation of the relative percentages of the *II Signal* with respect to the *III Signal*, obtained from the analysis of the spectra recorded at room temperature.

After the global EPR study, we found evidence of a specific coordination pattern in the structure of these dendrimers. First, we observed an interaction of Cu(II) with the internal core at a 1 : 1 ratio between the metal and the dendrimer balls. After saturation of the internal dendrimer sites at the core position, the external layers and surface groups become available for copper complexation. At this point, the vicinal ligands at the dendrimer internal/external layers are progressively

occupied by Cu^{2+} ions leading to strong spin–spin interactions which first give rise to a line broadening, then to exchange narrowing and, finally, to the spectrum disappearance. Finally, after saturating the external layers, the ions localize at the external surface, and at the highest Cu(II) concentrations, only water molecules are available for coordination.

Some other conclusions were extracted from the comparison of the behaviour between different dendrimer generations and different peripheral groups. We observed that, by increasing generation, more nitrogen sites are available for copper binding, without causing a strong repulsion between the charged ions, and a weaker (or simply more distorted) coordination with nitrogen sites was found. Moreover, the different interacting abilities of the dendrimers at different generations and as a function of copper concentration were quantified, and depend on different (a) void space, (b) branches flexibility, and (c) nitrogen site availability in the dendrimer core. If the comparison is performed between GnS and GnC dendrimers, we found a stronger complexation of Cu(II) with SO_3^- terminal groups with respect to CO_2^- peripheral groups. After and while coordinating the internal sites, the ions also interact with the close sulfonate groups by forming dimeric species.

All these results supported and extended the conclusions obtained by UV-Vis spectrophotometry, with respect to the geometry of the different coordination points in the dendritic structure. As we have demonstrated, both the dendritic skeleton and the surface groups play an important role in the coordination ability of the dendrimers, our polyanionic PPI dendrimers showing interesting differences compared to similar dendritic structures.

In relation to the dendritic skeleton, the behavior of our dendrimers is closer to that of PAMAM G1.5-CO_2Na[10] than to the dendrimer POSS-CO_2Na synthesized by Naka.[42]

According to spectrophotometric and isothermal titration calorimetric studies, Cu^{2+}–N_4 and Cu^{2+}–N_2O_2 complexes are possible coordination modes in the case of the PAMAM dendrimer depending on the ratio of the Cu^{2+}-dendrimer, while only the Cu^{2+}–N_2O_2 complex can be formed for POSS-CO_2Na, due to the conformation of the POSS-core dendrimer that causes the decrease in mobility of their chains. Further studies with earlier generations of carboxylate starbust PAMAM dendrimers[10] show a prevailing EPR signal due to a CuN_2O_2 coordination at intermediate pH. Meanwhile, we observed that PPI dendrimers present a preference for $CuNO_3$, probably arising from a more open structure which disfavours the coordination of the same copper ion between two branches.

The polyamino skeleton provides to our dendrimers an extended coordination ability, when compared to polyanionic carbosilane dendrimers previously synthesized by our group.[41] Moreover, copper ions can be included in the dendrimer cavities and surfaces in a controlled way, and final products remained water-soluble up to the highest copper dose. Some different components arise in the EPR spectra, especially in the case of sulfonate dendrimers, due to the different dendritic interior.

The role of the peripheral groups is as important as that performed by the dendritic skeleton. Previous studies have been performed on the uptake of Cu^{II} by poly(amidoamine) (PAMAM) dendrimers[5] with an EDA core in aqueous solutions with different terminal groups, such as primary amine, succinamic acid, glycidol, and acetamide. The overall results of the proton and metal ion binding measurements suggested that the uptake of Cu^{II} by these dendrimers involves both the dendrimer tertiary amines and terminal groups, but their extents of protonation control the ability of the dendrimers to bind Cu^{II}. Ottaviani *et al.* have carried out EPR studies[10,18] for PAMAM starbust dendrimers *n*SBD-NH_2 (n = 3, 5 and 7) and showed that 1 : 1 mixtures with Cu^{II} above pH 6 are exclusively bound to the exterior of the PAMAM structure, apparently due to the strong basicity and easy accessibility of the terminal primary amines; moreover, they demonstrated that dendritic cores for earlier generations can trap significant amounts of water which would also weakly coordinate the copper ions. Conversely, we established that the first Cu^{II} equivalent coordinates to the polyamine core of our polyanionic PPI dendrimers, specifically bound by nitrogen atoms; the contribution of water molecules bound to the dendritic structure becomes more important when increasing metal concentration, and according to the results for PAMAM dendrimers, they serve as high capacity chelating agents for metal ions.[18,43]

Conclusions

Polypropylene(imine) dendrimers with the ethylenediamino core of generations 1, 2 and 3 decorated with anionic carboxylate and sulfonate moieties have been synthesized and characterized. A specific pattern in the coordination of divalent metal ions was discovered, by means of UV-Vis and EPR spectroscopy, using Cu^{II} as a probe. The first equivalent is coordinated in the core of the dendrimer with a CuN_2O_2 geometry (*I Signal*), while the following equivalents are distributed in the structure in a precise way, mainly with $CuNO_3$ (*II Signal*) and CuO_4 (*III Signals*) geometries depending on the generation and terminal groups nature.

The possibility of generating different metal complexes from the same dendrimer and precisely knowing their structure is a great advantage in drug design.[6] Previous studies about unmodified PAMAM[5,44] and PPI[6] dendrimers showed that metal complexations preferably took place on the dendrimer surface. Such metal ion complexes could be partially destroyed by detoxifying agents in their transport through the blood stream. Thus, multifunctional dendrimers, capable of forming metal ion–intradendrimer complexes, as Appelhans[45,46] oligosaccharide shell dendrimers, or our polyanionic PPI with the EDA core can overcome those drawbacks.

Polyanionic peripheral groups clearly determine the coordination ability towards metal ions. An unmodified G3 PPI dendrimer with the DAB core[1] in MeOH was able to complex eight cations of Cu^{II}, Zn^{II} and Ni^{II} ions in the outer sphere by

the complexing unit of bis-(3-aminopropyl)amine. The analogous G3 glycodendrimer[21] complexed a similar amount of Cu^{II} in the dendritic scaffold, and nearly double the amount of Ni^{II}, due to physical encapsulation resulting from a weaker interaction with the dendritic polyamine scaffold compared with the strong binding of Cu^{II} in the scaffold.

In this paper, we demonstrate that polyanionic PPI dendrimers with the EDA core are able to complex a larger amount of copper ions, due to the anionic groups and the EDA core. This fact is probably extrapolated to other metal ions, such as nickel, cobalt or zinc, although further studies need to be done. Moreover, this potential coordination ability towards such metal ions will lead us to evaluate the antiviral properties of these compounds in future studies.

Experimental

General methods

Unless otherwise stated, reagents were obtained from commercial sources and used as received. ^{1}H, ^{13}C and ^{15}N NMR spectra were recorded on Varian Unity VXR-300 and Varian 500 Plus Instruments. Chemical shifts (δ, ppm) were measured relative to residual ^{1}H for water-d_2 and chloroform-d_1 used as solvents. For ^{13}C and ^{15}N external references were used. C, H and N analyses were carried out with a Perkin-Elmer 240C microanalyzer, and UV-Vis analyses with a UV-Vis Spectrophotometer Perkin-Elmer Lambda 18. The potentiometric titrations were performed using a CRISON titration system consisting of a digital potentiometer (pH-Meter BASIC 20+) and a pH electrode, which has an encapsulated reference system (*cartridge*) with an Ag^{+} ion barrier, two diaphragms and a CRISOLYT electrolyte. The pH meter was standardized at pH values 4.01, 7.00 and 9.21 using the appropriate buffer solutions.

EPR experiments

EPR spectra were analyzed using the programs NLSL, by Budil and Freed,[38] and the SimFonia, by Bruker (version 1.25). The first program was used to compute both room temperature and low temperature spectra, whereas the second one was only used to compute the low temperature spectra. The analysis provided the main components of the **g** tensor for the coupling between the electron spin and the magnetic field and of the **A** tensor for the coupling between the unpaired electron spin and the copper nuclear spin ($I = 3/2$; number of hyperfine lines = $2I + 1 = 4$). Furthermore, the computation of the spectra at room temperature also provided the correlation time for the rotational diffusion motion. The accuracy in the parameters resulting from computation is 2%, but it decreases for broad spectra (5%).

Dendrimers

Synthesis of polysulfonate dendrimers (7, 8, 9). In an ampoule, to a solution of polyamine in 3 mL of methanol, sodium vinylsulfonate (2 equiv. per amine group) was added. The solution was stirred for 48 h at 120 °C, then it was evaporated. The product was purified by nanofiltration devices for 1 day with cutoff membranes of MW = 500–1000 g mol^{-1}. The products were recovered by washing the membrane with water, and then evaporation, as white solids.

(**7**) Reactants: Dendrimer **2** (500 mg, 1.73 mmol), sodium vinylsulfonate (5.1 mL, 13.9 mmol) (2.1 g, 90%). $C_{30}H_{60}N_6Na_8O_{24}S_8$ (1329.3). δ_H (300 MHz, D_2O, 25 °C, TMS) 2.95 (m, 16 H, –NCH_2CH_2S–), 2.81 (20 H, m, –NCH_2CH_2S– and –$N(CH_2)_2$N–), 2.60 (8 H, m, –$^{c}NCH_2CH_2CH_2$–), 2.40 (8 H, m, –$^{c}NCH_2CH_2CH_2$–), 1.60 (8 H, m, –$^{c}NCH_2CH_2CH_2$–). δ_C (75 MHz, D_2O, 25 °C, TMS): δ = 52.8 (–$^{c}NCH_2CH_2CH_2$–), 51.0 (–$^{c}NCH_2CH_2CH_2$–), 50.3 (–$N(CH_2)_2N$), 47.6 (–NCH_2CH_2S–), 47.0 (–NCH_2CH_2S–), 22.0 (–$^{c}NCH_2CH_2CH_2$). HRMS (MALDI TOF): *m*/*z* calcd for $C_{30}H_{60}N_6Na_8O_{24}S_8-3Na^{+}$ + 2$H^{+}]^{-}$: 1261.31 $[M - 3Na^{+} + 2H^{+}]^{-}$; found: 1261.11.

(**8**) Reactants: Dendrimer **4** (500 mg, 0.67 mmol), sodium vinylsulfonate (3.93 mL, 10.7 mmol) (1.6 g, 85%). $C_{70}H_{140}N_{14}Na_{16}O_{48}S_{16}$ (2826.8). δ_H (300 MHz, D_2O, 25 °C, TMS) 2.89 (32 H, m, –NCH_2CH_2S–), 2.79 (52 H, m, –NCH_2CH_2S–, –$N(CH_2)_2$N– and –$CH_2NCH_2CH_2$S–), 2.39 (32 H, m, –$^{c}NCH_2CH_2CH_2$– and –$NCH_2CH_2CH_2$–), 1.65 (16 H, m, –$NCH_2CH_2CH_2$–), 1.54 (8 H, m, –$^{c}NCH_2CH_2CH_2$–). δ_C (75 MHz, D_2O, 25 °C, TMS) 51.0–50.0 (–$N(CH_2)_2$N–, –$^{c}NCH_2CH_2CH_2$–, –$NCH_2CH_2CH_2$–), 47.5 (–NCH_2CH_2S–), 47.0 (–NCH_2CH_2S–), 22.6 (–$^{c}NCH_2CH_2CH_2$), 21.1 (–$NCH_2CH_2CH_2$).

(**9**) Reactants: Dendrimer **6** (500 mg, 0.30 mmol), sodium vinylsulfonate (3.53 mL, 9.6 mmol) (1.4 g, 78%). $C_{150}H_{300}N_{30}Na_{32}O_{96}S_{32}$ (5821.9). δ_H (300 MHz, D_2O, 25 °C, TMS) 2.96 (64 H, m, –NCH_2CH_2S–), 2.84 (64 H, m, –NCH_2CH_2S–), 2.75–2.48 (116 H, m, –$N(CH_2)_2$N, –$^{c}NCH_2CH_2CH_2$– and –$NCH_2CH_2CH_2$–), 1.73 (40 H, m, –$^{c}NCH_2CH_2CH_2$– and –$NCH_2CH_2CH_2$–), 1.62 (16 H, m, –$NCH_2CH_2CH_2$–). δ_C (75 MHz, D_2O, 25 °C, TMS) 50.6–50.3 (–$N(CH_2)_2$N–, –$^{c}NCH_2CH_2CH_2$– and –$NCH_2CH_2CH_2$–), 47.4 (–NCH_2CH_2S–), 47.0 (–NCH_2CH_2S–), 22.0 (–$NCH_2CH_2CH_2$–), 21.9 (–$NCH_2CH_2CH_2$ and –$NCH_2CH_2CH_2$). HRMS (BIS-MMI-ESI): *m*/*z* calcd for $C_{150}H_{300}N_{30}Na_{32}O_{96}S_{32}-4Na^{+}$ + 5$H^{+}]^{+}$: 5734.96 $[M - 4Na^{+} + 5H^{+}]^{+}$; found: 5734.86.

Synthesis of polymethylester dendrimers (10, 12, 14). In an ampoule, to a solution of polyamine dendrimer in 5 mL of methanol, methyl acrylate (2.8 equiv. per amine group) was added. The solution was stirred at 80 °C for 18 h, then it was evaporated to eliminate all the volatiles. The products were isolated as yellow oils.

(**10**) Reactants: Dendrimer **2** (500 mg, 1.73 mmol), methyl acrylate (1.8 mL, 19.4 mmol) (1.6 g, 94%). $C_{46}H_{84}N_6O_{16}$ (977.19). δ_H (300 MHz, $CDCl_3$, 25 °C, TMS) 3.63 (24 H, s, CO_2Me), 2.73 (16 H, t, –$NCH_2CH_2CO_2Me$), 2.41 (36 H, m, –NCH_2–), 1.52 (8 H, m, –$NCH_2CH_2CH_2N$–). δ_C (75 MHz, $CDCl_3$, 25 °C, TMS) 173.0 (CO_2Me), 52.5, 52.4, 51.8 (–NCH_2–), 51.5 (CO_2Me), 49.1 ($NCH_2CH_2CO_2Me$), 32.4 ($NCH_2CH_2CO_2Me$), 24.7 (–$NCH_2CH_2CH_2N$–).

(**12**) Reactants: Dendrimer **4** (500 mg, 0.67 mmol), methyl acrylate (1.4 mL, 15.0 mmol) (1.2 g, 90%). $C_{98}H_{182}N_{14}O_{28}$ (2004.6). δ_H (300 MHz, $CDCl_3$, 25 °C, TMS) 3.64 (48 H, s, CO_2Me), 2.74 (32 H, t, –$NCH_2CH_2CO_2Me$), 2.41 (84 H, m,

–NCH_2–), 1.52 (24 H, m, –NCH$_2$CH_2CH$_2$N–). δ_C (75 MHz, $CDCl_3$, 25 °C, TMS) 173.0 (CO_2Me), 52.0–51.5 (–NCH_2–), 51.5 (CO_2Me), 49.2 (N$CH_2CH_2CO_2$Me), 32.4 (NCH$_2$$CH_2CO_2$Me), 24.6 (–NCH$_2$$CH_2CH_2$N–).

(**14**) Reactants: Dendrimer **6** (500 mg, 0.30 mmol), methyl acrylate (1.2 mL, 13.4 mmol) (1.0 g, 78%). $C_{214}H_{396}N_{30}O_{64}$ (4413.6). δ_H (300 MHz, $CDCl_3$, 25 °C, TMS) 3.63 (96 H, s, CO_2Me), 2.73 (64 H, m, –NC$H_2CH_2CO_2$Me), 2.41 (180 H, m, –NCH_2–), 1.52 (56 H, m, –NCH$_2$CH_2CH$_2$N–).

Synthesis of polycarboxylate dendrimers (11, 13, 15). A solution of sodium hydroxide (1.1 equiv. per carboxylate group) in MeOH was added to the polymethylester dendrimer dissolved in MeOH and they were stirred at room temperature for 24 h. The product was isolated under vacuum, dissolved in water and purified through nanofiltration devices for 1 day with cut-off membranes of MW = 500–1000 g mol^{-1}. Pure products were isolated as white microcrystalline solids, after evaporation to dryness and washing with diethyl ether.

(**11**) Reactants: Dendrimer **10** (500 mg, 0.51 mmol), NaOH (180 mg, 4.5 mmol). (520 mg, 98%) $C_{38}H_{60}N_6Na_8O_{16}$ (1040.83). δ_H (300 MHz, D_2O, 25 °C, TMS) 2.56/2.55* (16 H, m, –NC$H_2CH_2CO_2$Na, protonated*), 2.42 (4 H, s, –N(CH$_2$)$_2$N–), 2.32 (8 H, m, –^{c}NC$H_2CH_2CH_2$N–), 2.26/2.35* (8 H, m, –^{c}NCH$_2$CH$_2$CH_2N–, protonated*), 2.18 (16 H, m, –NCH$_2$CH_2CO_2Na), 1.45 (8 H, m, –^{c}NCH$_2$CH_2CH$_2$N–). δ_C (75 MHz, D_2O, 25 °C, TMS) 181.5/180.3* (CO_2Na, protonated*), 53.7 (–^{c}N$CH_2CH_2CH_2$N–), 49.9 and 49.8/46.0* (–N(CH$_2$)$_2$N–, and N$CH_2CH_2CO_2$Na, protonated*), 37.5 (NCH$_2$$CH_2CO_2$Na), 24.0 (–NCH$_2$$CH_2CH_2$N–).

(**13**) Reactants: Dendrimer **12** (500 mg, 0.25 mmol), NaOH (176 mg, 4.4 mmol). (540 mg, 96%). $C_{86}H_{140}N_{14}Na_{16}O_{32}$ (2250.0). δ_H (300 MHz, D_2O, 25 °C, TMS) 2.55 (32 H, m, –NC$H_2CH_2CO_2$Na), 2.41 (4 H, s, –N(CH$_2$)$_2$N–), 2.24 (48 H, m, –NC$H_2CH_2CH_2$N–), 2.14 (32 H, m, –NCH$_2$CH_2CO_2Na), 1.44 (24 H, m, –NCH$_2$CH_2CH$_2$N–).

(**15**) Reactants: Dendrimer **14** (500 mg, 0.11 mmol), NaOH (160 mg, 4.0 mmol) (488 mg, 95%). $C_{182}H_{300}N_{30}Na_{32}O_{64}$ (4668.2). δ_H (300 MHz, D_2O, 25 °C, TMS) 2.56 (64 H, m, –NC$H_2CH_2CO_2$Na), 2.41 (4 H, s, –N(CH$_2$)$_2$N–), 2.25 (112 H, m, –NC$H_2CH_2CH_2$N–), 2.15 (64 H, m, –NCH$_2$CH_2CO_2Na), 1.45 (56 H, m, –NCH$_2$CH_2CH$_2$N–).

Acknowledgements

This work has been supported by grants from ME&C (Ref. CTQ2011-23245), Consortium NANODENDMED ref. S2011/BMD-2351 (CAM) and Proyecto CAM-UAH 2011 (Reference UAH2011/EXP-037) to University of Alcalá. This work was supported by grants from the Consejería de Educación de la Comunidad de Madrid and Fondo Social Europeo (F.S.E.) for S.G.G. CIBER-BBN is an initiative funded by the VI National R&D&i Plan *2008–2011, Iniciativa Ingenio 2010, Consolider Program, CIBER Actions* and financed by the Instituto de Salud Carlos III with assistance from the *European Regional Development Fund*.

References

1 A. W. Bosman, H. M. Janssen and E. W. Meijer, *Chem. Rev.*, 1999, **99**, 1665–1688.
2 U. Boas and P. M. H. Heegaard, *Chem. Soc. Rev.*, 2004, **33**, 43–63.
3 A. Agarwal, S. Saraf, A. Asthana, U. Gupta, V. Gajbhiye and N. K. Jain, *Int. J. Pharm.*, 2008, **350**, 3–13.
4 C. Saudan, V. Balzani, M. Gorka, S.-K. Lee, J. van Heyst, M. Maestri, P. Ceroni, V. Vicinelli and F. Vögtle, *Chem.–Eur. J.*, 2004, **10**, 899–905.
5 M. S. Diallo, S. Christie, P. Swaminathan, L. Balogh, X. Shi, W. Um, C. Papelis, W. A. r. Goddard and J. H. J. Johnson, *Langmuir*, 2004, **20**, 2640–2651.
6 A. W. Bosman, A. P. H. J. Schenning, R. A. J. Janssen and E. W. Meijer, *Chem. Ber.*, 1997, **130**, 725–728.
7 E. C. Wiener, F. P. Auteri, J. W. Chen, M. W. Brechbiel, O. A. Gansow, D. S. Schneider, R. L. Belford, R. B. Clarkson and P. C. Lauterbur, *J. Am. Chem. Soc.*, 1996, **118**, 7774–7782.
8 T. Pietsch, N. Cheval, D. Appelhans, N. Gindy, B. Voit and A. Fahmi, *Small*, 2011, **7**, 221–225.
9 O. Yemul and T. Imae, *Colloid Polym. Sci.*, 2008, **286**, 747–752.
10 M. F. Ottaviani, S. Bossmann, N. J. Turro and D. A. Tomalia, *J. Am. Chem. Soc.*, 1994, **116**, 661–671.
11 M. Zhao, L. Sun and R. M. Crooks, *J. Am. Chem. Soc.*, 1998, **120**, 4877–4878.
12 P. J. Pellechia, J. Gao, Y. Gu, H. J. Ploehn and C. J. Murphy, *Inorg. Chem.*, 2004, **43**, 1421–1428.
13 F. Tarazona-Vasquez and P. B. Balbuena, *J. Phys. Chem. B*, 2005, **109**, 12480–12490.
14 K. A. Krot, A. F. D. de Namor, A. Aguilar-Cornejo and K. B. Nolan, *Inorg. Chim. Acta*, 2005, **358**, 3497–3505.
15 R. M. Crooks, M. Zhao, L. Sun, V. Chechik and L. K. Yeung, *Acc. Chem. Res.*, 2000, **34**, 181–190.
16 L. Zhou, D. H. Russell, M. Zhao and R. M. Crooks, *Macromolecules*, 2001, **34**, 3567–3573.
17 M. S. Diallo, L. Balogh, A. Shafagati, J. H. Johnson Jr., W. A. Goddard III and D. A. Tomalia, *Environ. Sci. Technol.*, 1999, **33**, 820–824.
18 M. F. Ottaviani, F. Montalti, N. J. Turro and D. A. Tomalia, *J. Phys. Chem. B*, 1997, **101**, 158–166.
19 M. Zhao and R. M. Crooks, *Chem. Mater.*, 1999, **11**, 3379–3385.
20 M. F. Ottaviani, R. Valluzzi and L. Balogh, *Macromolecules*, 2002, **35**, 5105–5115.
21 D. Appelhans, U. Oertel, R. Mazzeo, H. Komber, J. Hoffmann, S. Weidner, B. Brutschy, B. Voit and M. F. Ottaviani, *Proc. R. Soc. London, Ser. A*, 2010, **466**, 1489–1513.
22 M. F. Ottaviani, F. Montalti, M. Romanelli, N. J. Turro and D. A. Tomalia, *J. Phys. Chem.*, 1996, **100**, 11033–11042.
23 M. F. Ottaviani, P. Favuzza, M. Bigazzi, N. J. Turro, S. Jockusch and and D. A. Tomalia, *Langmuir*, 2000, **16**, 7368.

24 N. J. Turro, W. Chen and M. F. Ottaviani, in *Dendrimers and other dendritic polymers*, ed. J. M. J. F.-D. A. Tomalia, John Wiley & Sons Ltd, 2002, p. 309.
25 M. F. Ottaviani and N. J. Turro, *Advanced ESR methods in polymer research*, 2006, pp. 279–306.
26 K. Vassilev and W. T. Ford, *J. Polym. Sci., Part A: Polym. Chem.*, 1999, **37**, 2727–2736.
27 K. Vassilev, S. Turmanova, M. Dimitrova and S. Boneva, *Eur. Polym. J.*, 2009, **45**, 2269–2278.
28 M. S. Refat, I. M. El-Deen, I. Grabchev, Z. M. Anwer and S. El-Ghol, *Spectrochim. Acta, Part A*, 2009, **72**, 772–782.
29 B. A. Jansen, J. v. d. Zwan, J. Reedijk, H. d. Dulk and J. Brouwer, *Eur. J. Inorg. Chem.*, 1999, **9**, 1429–1433.
30 N. Malik, E. G. Evagorou and R. Duncan, *Anti-Cancer Drugs*, 1999, **10**, 767–776.
31 S. García-Gallego, M. J. Serramía, E. Arnaiz, L. Díaz, M. A. Muñoz-Fernández, P. Gómez-Sal, M. F. Ottaviani, R. Gómez and F. J. de la Mata, *Eur. J. Inorg. Chem.*, 2011, 1657–1665.
32 S. García-Gallego, J. Sánchez Rodríguez, J. L. Jiménez, M. Cangiotti, M. F. Ottaviani, M. A. Muñoz-Fernández, R. Gómez and F. J. de la Mata, *Dalton Trans.*, 2012, **41**, 6488–6499.
33 C. Valério, J. Ruiz, E. Alonso, P. Boussaguet, J. Guittard, J.-C. Blais and D. Astruc, *Bull. Soc. Chim. Fr.*, 1997, **134**, 907–914.
34 H.-C. Liang, S. K. Das, J. R. Galvan, S. M. Sato, Y. Zhang, L. N. Zakharov and A. L. Rheingold, *Green Chem.*, 2005, **7**, 410–412.
35 R. C. Van Duijvenbode, A. Rajanayagam and G. J. M. Koper, *Macromolecules*, 2000, **33**, 46–52.
36 Z. Qiang and C. Adamas, *Water Res.*, 2004, **38**, 2874–2890.
37 *Marvin, Calculator Plugin and Chemical Terms Demo*m http://www.chemaxon.com/marvin/sketch/index.jsp
38 D. E. Budil, S. Lee, S. Saxena and J. H. Freed, *J. Magn. Reson., Ser. A*, 1996, **120**, 155–189.
39 H. Wan, S. Li, T. A. Konovalova, S. F. Shuler, D. A. Dixon and S. C. Street, *J. Phys. Chem. C*, 2008, **112**, 1335–1344.
40 H. Wan, S. Li, T. A. Konovalova, Y. Zhou, J. S. Thrasher, D. A. Dixon and S. C. Street, *J. Phys. Chem. C*, 2009, **113**, 5358–5367.
41 M. Galán, J. Sánchez Rodríguez, M. Cangiotti, S. García-Gallego, J. L. Jiménez, R. Gómez, M. F. Ottaviani, M. A. Muñoz-Fernández and F. J. de la Mata, *Curr. Med. Chem.*, 2012, **19**, 4984–4994.
42 K. Naka, M. Fujita, K. Tanaka and Y. Chujo, *Langmuir*, 2007, **23**, 9057–9063.
43 S.-T. Lin, P. K. Maiti and W. A. Goddard III, *J. Phys. Chem. B*, 2005, **109**, 8663–8672.
44 R. M. Crooks, B. I. Lemon III, L. Sun, L. K. Yeung and M. Zhao, *Top. Curr. Chem.*, 2001, **212**, 81–135.
45 D. Appelhans, Y. Zhong, H. Komber, P. Friedel, U. Oertel, U. Scheler, N. Morgner, D. Kuckling, S. Richter, J. Seidel, B. Brutschy and B. Voit, *Macromol. Biosci.*, 2007, **7**, 373–383.
46 B. Klajnert, D. Appelhans, H. Komber, N. Morgner, S. Schwarz, S. Richter, B. Brutschy, M. Ionov, A. K. Tonkikh, M. Bryszewska and B. Voit, *Chem.–Eur. J.*, 2008, **14**, 7030–7041.